INTERNATIONAL ATOMIC ENERGY AGENCY
UNITED NATIONS EDUCATIONAL, SCIENTIFIC AND CULTURAL ORGANIZATION

INTERNATIONAL CENTRE FOR THEORETICAL PHYSICS
34100 TRIESTE (ITALY) - P.O.B. 586 - MIRAMARE - STRADA COSTIERA 11 - TELEPHONE: 2240-1
CABLE: CENTRATOM - TELEX 460392 - I

SECOND WORKSHOP ON OPTICAL FIBRE COMMUNICATION

(14 - 25 March 1988)

SEMINARS PRESENTED BY THE PARTICIPANTS

JAADA Ali

Abstract : Numerical simulation to calculate loss in optical coupler.

1) I will do a description of the structure wich are studied in my laboratory, and I will expose the mathematical problem.

2) I will discuss about the mathematical problem in unbounded and bounded domain. I will discuss too about Green function wich is a very important function in our problem.

3) I will expose the actual state of the simulation, and what happen in the future.

2

THE USE OF OPTICAL FIBERS IN THE TRANSMISSION OF IMAGES

A.Tagliaferri,C.J.Lopes,J.Nagai (Universidade Federal Fluminense-Brazil) and J.Calatroni (Universidad Simón Bolivar-Venezuela)

Fibers can be used to transmit optical images. Because de geometrical diferenc es beetween the signal to be transmitted and the channel, it is necessary to adapt the fibers to the signal or the signal to the fiber. In the first case are used 2-D arrays of fibers (endoscopes), in wich each fiber transmit a portion of the image. In the second case it is posible to adapt the image to the fiber by pure optical means, using the so called "Chromatic codification".
We present here some results of ouer experiments on the transmission of images via chromatic codification

Realization of the refracted near field method

I. P. Mahai

Research Institute for Technical Physics (Hungary)

In this paper a technical solution of the measurement of the refracting index profile using the refracted near field method will be discussed. Some intercomparison between the results of this method and the near field method will be shown on MM fibres.

"100-FOLD COMPRESSION OF YAG:Nd^{3+} LASER PULSES USING SINGLEMODE OPTICAL FIBERS"

ABSTRACT

Telma V. Cardoso, Marcia T. Portela, Valeria L. da Silva, and C.H. Brito Cruz
INSTITUTO DE FISICA
DEPARTAMENTO DE ELETRONICA QUANTICA
UNIVERSIDADE ESTADUAL DE CAMPINAS
13.100 CAMPINAS SP BRAZIL

We will discuss and present results on the compression of 120 ps pulses from a YAG:Nd^{3+} laser to 1.4 ps. The pulse compression technique employs a singlemode optical fiber and a dispersive delay line composed of a grating pair. Upon propagation through the 1.8 km fiber, the pulses from the YAG laser are spectrally broadened to 30 A and assume a flat topped temporal profile. The grating pair provides the necessary negative group velocity dispersion to compress the chirped pulse emerging from the fiber. The average power coupled into the fiber is 300 mW.

We will discuss briefly the pulse compression technique, based on the self-phase modulation effect that, together with the positive group velocity dispersion of the fiber, is responsible for the spectral broadening. The negative group velocity dispersion of the grating pair is adjusted changing the gratin, distance. This grating distance, plotted against the compressed time duration pulses, presents an optimum value , where the compressed pulse is shorter.

PRISM COUPLING TECHNIQUE FOR THE MEASUREMENT OF THE MODE SPECTRA OF OPTICAL FIBERS

12

K. THYAGARAJAN, M.R. SHENOY AND M.R. RAMADAS
Department of Physics
Indian Institute of Technology
NEW DELHI - 110 016.

ABSTRACT

We present the prism coupling technique for the measurement of mode spectra of optical fibers. Experimental results on the measurement of propagation constant in a normal single-mode fiber and the application of this technique to the measurement of beat length in birefringent optical fibers is presented.

HIGH FREQUENCY ELECTRONICS FOR TERRESTRIAL AND SATELLITE COMMUNICATIONS

13

JOSE LUIS MEDINA MONROY
CICESE RESEARCH CENTER
ENSENADA B.C, MEXICO

ABSTRACT

THIS WORK DESCRIBES THE DESIGN AND FABRICATION TECHNIQUES OF SOLID STATE MICROWAVE COMPONENTS USING GALLIUM ARSENIDE FIELD EFFECT TRANSISTOR AS ACTIVE DEVICE. THE APPLICATION OF THESE COMPONENTS ARE ON SATELLITE AND TERRESTRIAL COMMUNICATIONS SYSTEMS WICH WORKS AT MICROWAVE FREQUENCIES (C AND KU BAND).

ABSTRACT

A Fiber-Optic Sagnac interferometer for rotation sensing is described. The system utilizes a 100 m long, single mode fiber ($\lambda = 6330$ Å) and is mounted on top of an automatic rotating drum. This permitts the complete characterization of the sensor.

A stabilized and frequency locked HeNe laser is used to launch a beam into the two ends of the fiber. A piezoeletric modulator operating at the frequency of 30 Khz and a silicon pin photodetector complete the detection system.

A.A.P.Poll and M.T.T.Pacheco

- Laser Division, Brazilian Airspace Technical Center -

S.J.Campos - S.P. - Brazil

P. Díaz, C. González

Laboratorio de Investigaciones en Electrónica del Estado Sólido. Facultad de Física. Universidad de La Habana.

GaP - $Al_xGa_{1-x}P$ Heterostructure Edge Coupling Waveguides for Hybrid Integrated - Optic Devices.

Abstract :

In this paper we present the performance of GaP - $Al_xGa_{1-x}P$ heterostructure waveguides for integrated - optic hybrid devices. The waveguide layer is grated with a parabolic refractive index profile for the light emission of a DH - GaAs semiconductor laser. The waveguide heterostructure performed allows to couple at it edge cross - section semiconductor laser or photodetector as well as fi.. or soldier them on the same substrate over which the heterostructure layers were deposited.

The heterostructure layers were grown by liquid - phase epitaxy and the heterostructure waveguide was performed by means of etching technics specially developed for this purpose.

Both, the growth procedure, as well as the etching technics are described. The results achieved are shown in curves and photographies, taken on a scanning microscope.

P. Gomes, G. Barreira, T. Almeida (LIP-Lisbon)
P. Alves, P. Leite (INESC-Porto)
E. Gerelle (DEC), R. A. McLaren (CERN)

SUMMARY

The next generation of experiments at CERN (LEP) will have a distance of up to 300m between the data acquisition computers and the FASTBUS crate near the detectors.

Two ways of satisfying this requirement were considered: a FASTBUS to FASTBUS link, transmitting the System Interconnect protocol, or providing an optical extension for the CERN Host Interface (CHI). The latter implementation was chosen as it has the advantage of not being dedicated to FASTBUS and is simpler to implement.

The optical interconnect provides a general purpose, full duplex, link with a bandwidth of 10 Mbytes/sec over distances up to 1000 meters. It has been designed to be transparent to software (except on the occurence of a reset).

Handshake delays have been minimised by pipelining. A fifo at the receive end buffers the incoming data. Data flow control is provided by a stop/go status bit which informs the transmitter that the receiver fifo is three-quarters full; the transmitter must then stop sending until the receiver fifo signals that is prepared to accept further data.

The signals entering the Optical Interconnect are split into three groups: data, control, and status. These are serialised and transmitted over a pair of fibers and recovered into standard signals at the receiver end.

The Advanced Micro Devices TAXI pair is used to serialise each byte into a bit stream and recover it after transmission through the fiber. Tests on these components are being performed in several laboratories, including INESC-Porto. In addition, the fiber and electro-optical transducers were also tested. A report on the final results will be presented.

The present implementation is not restricted to applications linking VAX computers to FASTBUS but can also provide long distance connections from FASTBUS to FASTBUS, VAX to VAX computers or VMEbus to VMEbus.

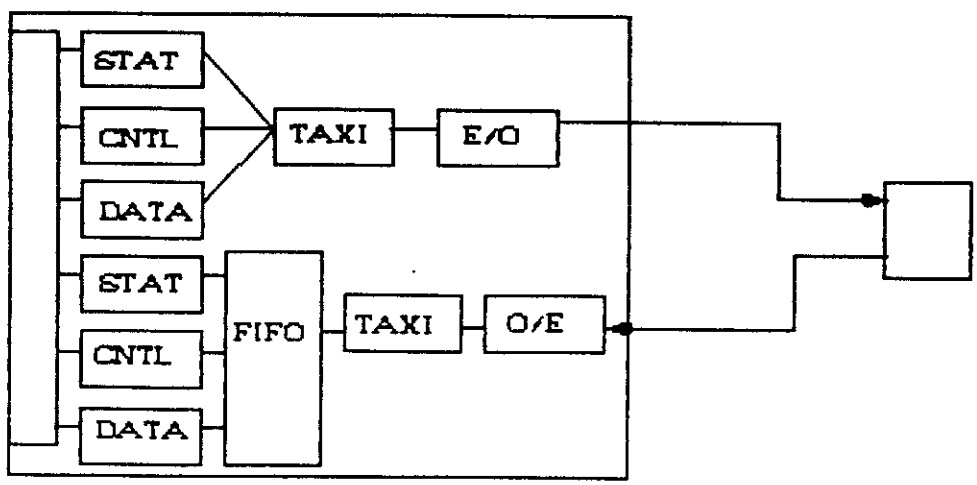

GEOMETRICAL CHARACTERIZATION OF LIQUID CORE FIBERS BY MEASUREMENT OF THERMALLY INDUCED MODE CUTOFFS AND INTERFERENCE.

Susanne [illegible], Erich [illegible], [illegible] Srivastava

Transmitted and scattered intensity in liquid core fibers have been measured as a function of temperature and v values of cutoff points obtained.
The measurement of the period of the oscillations in the transmitted intensity can be used to make high precision non destructive measurements of core radius and core ellipticity along the fiber length.

Internal Seminar, Contribution

Title: An Easy Approach to Design of Digital Optical links

Author: Raimundo Duarte (Brazil)
(Please After Next Friday - 21st Ideal)

Abstract: ~~It~~

This work presents a straightforward method to design digital optical links, considering all relevant ~~aspects~~ parameters of each system ~~com~~ component, say, sources, detectores and fibers itself. An Efford is made to take in account all aspects concerned with a real system.

(Time About 30 minutes)

ANALYSIS OF FIBER DIRECTIONAL COUPLER WITH A BUFFER LAYER

Anurag Sharma and Prasanna K. Mishra*
Physics Department, Indian Institute of Technology Delhi,
New Delhi-110016, INDIA

Single mode fiber directional couplers made by mechanical lapping (also known as polished couplers) have lately been a subject of great interest[1-3] as they are more durable and stable and are continuously tunable. The unavoidable space ($\sim$ 0.1-0.2 micron thick) between the two substrate blocks containing the fiber is usually filled with some index matching liquid. It is also possible to introduce a buffer layer of a material with suitable properties to alter the coupling length externally as desired.

The analysis of directional couplers is usually based on coupled mode theory[4] which gives an approximate analytical expression for the coupling length. However, using this approach, it would be extremely difficult to study the effect of a buffer layer. We have developed a simple model for directional couplers which gives good accuracy and allows one to study the effect of a buffer layer. The model is based on finding a dielectric slab directional coupler which is approximately equivalent to the fiber coupler. The analysis is similar to the one which we have developed for rectangular waveguides & directional couplers[5]. We have then extended the exact analysis of slab directional couplers[6] to include the effect of a buffer layer. The equivalent coupling geometry thus provides a

---

* Present address: G.M.College, Sambalpur, Orissa (India).

simple means to study the coupling characteristics of a practical fiber coupler.

The accuracy of the model is illustrated in Fig.1 where we have plotted the normalised coupling coefficient as a function of separation of two fibers using the coupled mode theory with exact modal field and using our method. The agreement is within 5%. In Fig.2, we have plotted, as an example, the coupling length as a function of the refractive index & thickness of the buffer layer for a typical directional coupler with parameters given on the figure. Further studies are in progress and the results will be reported at the conference.

References:

1. Bergh, R.A., et al., Electron Lett. 16, 260 (1980)
2. Parriaux , O., et al., Appl. Opt. 20, 2420 (1981)
3. Digonnet, M.J.F., Opt. Lett. 10, 463 (1985)
4. Snyder, A.W., J.Opt. Soc.Am. 62, 1267 (1972)
5. Sharma, et al., Proc. 'Second European Conference on Integrated Optics', 17-18 Oct. 1983,Florence (Italy), IEE Conf. Publication No.227, p.9
6. Kapany, NS & Burke, J.J., 'Optical Waveguides' (Academic Press, 1971).

Captions

Fig 1: Normalised coupling coefficient $\tilde{\kappa}$ $\left[\pi a/(2 L_c \sqrt{\Delta}) \quad ; \quad \Delta = (n_o^2 - n_s^2)/2 n_o^2\right]$ as a function of normalised separation, d/a, for step-index fiber directional couplers.

Fig. 2: The coupling length, L_c , as a function of the refractive index of the buffer layer for step-index fiber directional couplers with n_o = 1.46 n_s = 1.4569 a = 2.26 μm , λ = 0.6328 μm.

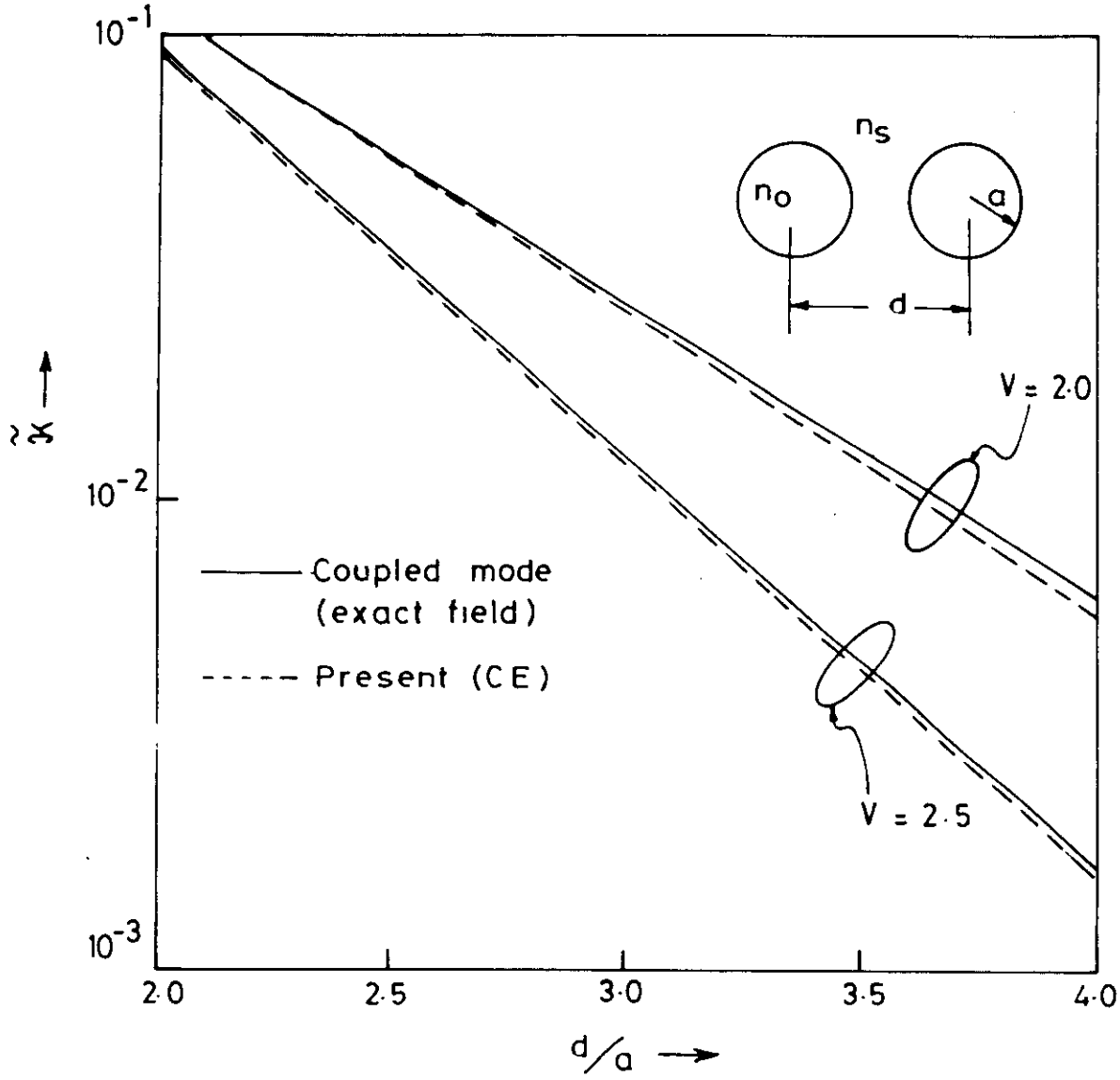
10^{-1}
10^{-2}
10^{-3}
κ
n_s
n_o
a
d
V = 2·0
V = 2·5
Coupled mode
(exact field)
Present (CE)
2·0
2·5
3·0
3·5
4·0
d/a

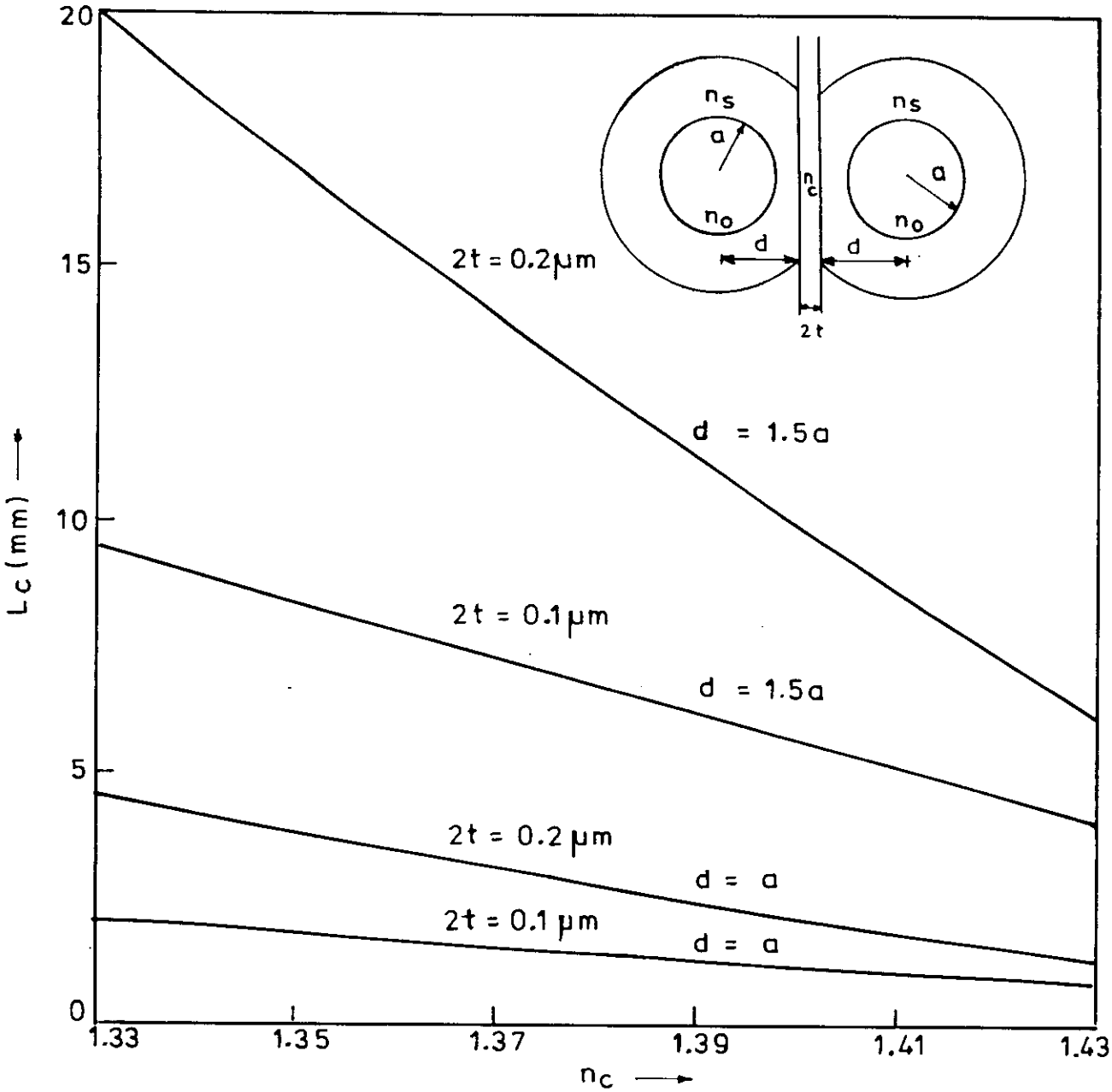
20
15
10
5
0
Lc (mm) ⟶
1.33
1.35
1.37
1.39
1.41
1.43
nc ⟶
2t = 0.2μm
d = 1.5a
2t = 0.1μm
d = 1.5a
2t = 0.2 μm
d = a
2t = 0.1 μm
d = a
ns
a
no
nc
d
2t

International Atomic Energy Agency
and
United Nations Educational Scientific and Cultural Organization
INTERNATIONAL CENTRE FOR THEORETICAL PHYSICS

THE SPONTANEOUS EMISSION FACTOR FOR SEMICONDUCTOR INJECTION LASER

Yiguang Zhao and Changzhi Guo

Department of Physics, Peking University, Beijing, China.

ABSTRACT

In this paper, The relations between the spontaneous emission factor and the laser structure, waveguide mechanism, working condition etc. were investigated both on theory and experiments. The results show that the shorter the cavity length and the narrower the stripe width, the larger the spontaneous emission factor is. The spontaneous emission factor has the maximum value, when the thickness of the active layer is about 0.2μm . In a small region under the threshold, the spontaneous emission factor increases quickly as the injected current increases and outside this region, the variation of this factor is small. The difference between the spontaneous emission factor of the main mode and the neighbouring modes is small,but there is a large difference between spontaneous emission factor of the main mode and the side mode which is far from the main mode. The spontaneous emission factor of InGaAsP BH lasers is larger than that of AlGaAs stripe geometry lasers

I. INTRODUCTION

The spontaneous emission factor is an important parameter of semiconductor lasers . It is defined by the ratio of the amount of the spontaneous light emission into a specific laser mode to the amount of total spontaneous emission. Since it determines the spectral and dynamic features of a laser [1,3] therefore a lot of attention has been paid to it. Up to now, factors which influence the value of the spontaneous emission factor have been studied theoretically [4,5,6], and several methods to measure this factor have been established [7,8]. In [6], various theories about the spontaneous emission factor have been analyzed and compared. The results show that K.Petermann's theory is more appropriate than other theories. It is necessary to do further research to make the relations between the value of the spontaneous emission factor and the laser structure, waveguide mechanism and working conditions etc. clear. Morever the relations between this factor and the injected current has not yet been investigated, and up to now the spontaneous emission factor has been treated as a constant. So clearing these relations is very significant for understanding the characteristics of the laser, and designing a laser.

There are two methods to measure the spontaneous emission factor. The first one is to measure the optical output versus the injected current and to compare with theoretical predictions at various values of the spontaneous emission factor[7]. This method has a large error. A more accurate one is the harmonic measurement method [8]. But in [8], because the relation between the gain coeficient and the injected carrier density was approximately given by $g(y)\cong a'n(y)$ and effects of the transparent carrier density and laser wavelength were ignored. Therefore it is certain to cause error, especially for the side mode which is far from the main mode.

In this paper, based on [6], the relations between the spontaneous emission factor and the laser structure, waveguide mechanism and working conditions were obtained from deriving a self-consistent solution of the optical field equation and diffusion equation. Using the harmonic measurement method, all factors which influence the gain were consisdered. The spontaneous emission factor was investigated for the AlGaAs stripe geometry and the InGaAsP BH laser , Using spline fit and successive iterations, the relation between the spontaneous emission factor and the injected current was obtaind. The experimental results are in agreement with theoretical calculation.

II. THEORY ANALYSIS AND NUMERICAL RESULTS

If the spontanous emission is treated as the radiation of arbitrarily oriented uncorrelated electric dipoles within the active layer. Its optical fields are expanded in a series of the guiding mode. So the spontaneons emission factor is given by [5].

$$C=\frac{\lambda^4 K}{4\pi^2 \bar{n}_1 \bar{n}_2 \bar{N}mVe\ \Delta\lambda} \qquad (1)$$

Where λ is the laser wavelength.K is the astigmatism factor. $\bar{n}_1$ is the material refractive index in the active region. $\bar{N}m$ is the mode effective refractive index.

$$\bar{N}m=Re(\beta_z)/k_0 \qquad (2)$$

β_z is the complex propagation constant. k_0 is the wave number in the vacuum. $\bar{n}_e$ is the group refractive index [9]

$$\bar{n}_e=\bar{N}m-\lambda(d\bar{N}m/d\lambda) \qquad (3)$$

$$\frac{d\bar{N}m}{d\lambda}=\frac{1}{\bar{N}m}\left\{\Gamma\bar{n}_1\frac{\partial\bar{n}_1}{\partial\lambda}+(1-\Gamma)\bar{n}_2\frac{\partial\bar{n}_2}{\partial\lambda}\right\}+\frac{1}{\bar{N}m\lambda}\left\{\frac{\bar{n}_1-\bar{n}_2}{1+a(\bar{n}_1^2-\bar{n}_2^2)}-\frac{1}{a}\ln(1+a(\bar{n}_1^2-\bar{n}_2^2))\right\}$$

Γ is the confinemet factor with respect to the active layer. $\bar{n}_2$ is the material refractive index of the cladding layer. $a=(k_0 d)^2/2$, d is the thickness of the active layer.

Ve is effective volume of the active region. $Ve=L(d/\Gamma)We$, L is the cavity length, We is an effective laser width parallel to the active layer (y-direction).

$$We=\frac{\int|G(y)|^2dy\int Isp(y)dy}{\int|G(y)|^2Isp(y)dy} \qquad (4)$$

Where G(y) is the distribution of the modal optical field parallel to the active layer. Isp(y) is the distribution of the spontaneons emission parallel to the active layer, $Isp(y)\propto n(y)$. n(y) is the distribution of the carrier density in y-direction. $\Delta\lambda$ is the spontaneans emission spectral width. It depends on the injected cerrier density in the active region. For a laser with definite structure, when the carrier density reaches the threshold or goes above the threshold, the quasi-Fermi level does almost not change, and $\Delta\lambda$ also is almost fixed too. But the difference between the threshold currents of lasers with the different cavity length,the stripe width and the thickness of the active layer is very large. That means the difference between the quasi-Fermi levels of the electrons and the holes is very large at the threshold. Therefore $\Delta\lambda$ should change too.

The relation between the spontaneous emission spectral width and the gain spectral width $\Delta\lambda_g$ is approximatelly given by [10].

$$\Delta\lambda\cong 2\lambda_g \qquad (5)$$

The gain spectral width has approximately a linear relation with the injected carried density n. Based on the GaAs gain spectrum [11], a expression can be given by

$$\Delta\lambda_g=146.5\times10^{-18}n-95.4 \qquad (6)$$

Where the unit of the carrier density n is $1/cm^3$.

Under the threshold, the spontaneous emission spectral width increases as the bias current decreases. If GaAs is treaded as the homogeneous broadening medium, So the spontaneous emission

spectral width of a laser is given by [12]

$$\Delta\lambda = \Delta\lambda_r (1-u) \qquad (7)$$

$$u = \frac{2GL}{1-R1 \cdot R2}$$

Where $\Delta\lambda_r$ is the spectral width of the homogeneous broadening, and has a typical Value 400Å, G is the mode gain. R1 and R2 are the facet model power refrectivity.

Using the method which is the same as [6], a self-consistent solution of the optical field and diffusion equation was calculated. For the narrower stripe laser, the distribution of the injected current is supposed to be Gaussian form, and for the wide stripe laser it is supposed to be the distribution of a flat-top with the spreading sides . When the threshold condition was satisfied, the distribution of the optical field and the carrier density etc. were obtained from the self-consistent solution, at the same time. Then K-factor was calculated, the spontaneous emission factor was obtained from equation (1)-(7).

For the stripe geometry laser, the parameters which are same as [6] were given. The following results were obtained.

Fig.1 The spontaneous emission factor against the stripe width Sw, d=0.1μm, L=400μm, the ratio of the injected current to the threshold current is I/Ith=1.5

Fig.2 The spontaneous emissiom factor against the cavity length L. Sw=10μm, d=0.1μm. I/Ith=1.5

Fig.3 The spontaneous emission factor against the thickness of the active layer d, Sw=10μm, L=400μm, I/Ith=1.5

Fig.4 The spontaneous emission factor against the bias current I, d=0.1 μm, L=400 μm, Sw=10 μm.

Fig.1-4 illustrate the spontaneous emission factor of a stripe geometry laser operating at the fundumental mode . Fig.1 and 2 show that the spontaneous emission factor is a monotonically decreasing function of the stripe width and the cavity length. In Fig.3 the spontaneous emission factor has the maximum value at the thickness of the active layer being about 0.2μm . Fig.4 represents that in a certain region under the threshold, the spontaneous emission factor increases quickly as the injected current increases, and outside this region, its variation is small

For the buried heterostructure (BH) InGaAsP laser operating at 1.3μm wavelength, distributions of the optical field, the

carrier and the injected current are confined. The boundary conditions like [6] were given, K=1, C =2.5×10^{-4}were obtained. Where $\bar{n}$ =3.52, $\bar{n}_-$ =3.21, Sw=10μm, L=400μm.

III. EXPERIMENT

A. Principle

The rate equations of an injection semiconductor laser with multimode longitudinally is given by

$$\frac{dn}{dt} = \frac{j}{ed} - \frac{n}{\tau_s} - \sum_i g_i s_i \qquad (8)$$

$$\frac{ds_i}{dt} = g_i s_i - \frac{s_i}{\tau_{pi}} + C_i \frac{n}{\tau_s} \qquad (9)$$

Where j is the injected current density, e is the electronic charge. s_i is the photon density of the ith mode. C_i is the spontaneous emission factor of the ith mode. τ_{pi} is the photon lifetime. g_i is the gain coefficient of the ith mode. It depends on not only the carrier density, but also the wavelength of the longitudinal mode. If two quantities can approximately be considered as separable, then the gain spectrum is approximately given as a Loretzian line form [13]

$$g_i = va'(n-n_e)\left[1-4\left(\frac{\lambda_i-\lambda_0}{\Delta\lambda}\right)^2\right] \qquad (10)$$

Where v is the optical velocity in the active region, a' is the gain constant. n_e is the transparent carrier density. $\Delta\lambda$ is the full width of the gain spectrum, λ_0 is the wavelength of the main mode. λ_i is the wavelength of the ith mode. Define

$$M_l = \frac{\sum_i g_i s_i}{g_l s_l} = \frac{\sum_i \left[1-4\left(\frac{\lambda_i-\lambda_0}{\Delta\lambda}\right)^2\right] s_i}{\left[1-4\left(\frac{\lambda_l-\lambda_0}{\Delta\lambda}\right)^2\right] s_l} \qquad (11)$$

Inserting (10) and (11) into (8) and (9), and solving for the steady state produces

$$s_l(J) = \frac{J+NeM_l - Q+\sqrt{(Q-J-NeM_l)^2+4M_l JC_l}}{2DM_l} \qquad (12)$$

where $J=a'vB\tau_s\tau_{pl}j/ed$ $\quad Ne=a'vBn_e C_l\tau_{pl}$

$Q=a'vBn_e\tau_{pl}+1$

$D=a'vB\tau_s$ $\quad B=1+4\left(\frac{\lambda_l-\lambda_0}{\Delta\lambda}\right)^2$

set $f(t)=J+NeM_l - Q+\sqrt{(Q-J-NeM_l)^2+4M_l JC_l}$ (13)

obviously, M_l is a function of the normalized current J. If the spontaneous emission factor changes with the injected current, it should be a function of J too. Firstly only M_l is considered as the function of J. The derivative of the C_l to J is temporarily treaded as zero. Then one obtained

$$f'(J)=1+NeM_l' +Y/W \qquad (14)$$

$$f''(J)=NeM_l'' +Z/W-Y^2/W^3 \qquad (15)$$

$$f'''(J)=NeM_j'''+R/W-3ZY/W^3+3Y^3/W^5 \qquad (16)$$

where

$$W=\sqrt{(Q-J-NeM_j)^2+4M_j JC_j}$$

$$Y=J-Q+(Ne+2C_j)M_j+(NeJ+Ne^2M_j-QNe+2C_jJ)M_j'$$

$$Z=1+(2Ne+4C_j)M_j'+Ne^2(M_j')^2+(NeJ+Ne^2M_j-QNe+2C_jJ)M_j''$$

$$R=3Ne^2M_i'M_i''+(3Ne+6C_j)M_j''+(NeJ+Ne^2M_j-QNe+2C_jJ)M_j'''$$

The following expression can be obtained from equation (12):

$$s_i'(J)=[f'(J)/M_i-f(J)M_i'/M_i^2]/2D \qquad (17)$$

$$s_i''(J)=[f''(J)/M_i-2M_i'f'(J)/M_i^2+2f(J)(M_i')^2/M_i^3-f(J)M_i''/M_i^2]/2D \qquad (18)$$

$$s_i'''(J)=[f'''(J)/M_i-(3f''(J)M_i'+3f'(J)M_i''+f(J)M_i''')/M_i^2+(6f'(J)(M_i')^2+6f(J)M_i'M_i'')/M_i^3-6f(J)(M_i')^3/M_i^4]/2D \qquad (19)$$

Using the harmonic measurement method, if the ratio of the peak value of modulation signal to the bias current was supposed to be m (m is the modulation index). The peak values of the first and the second harmonics are A1 and A2 respectively. Then

$$A1/A2=4s_i'(J)/ms_i''(J) \qquad (20)$$

A series longitudinal mode spectrum were scaned from the below threshold to the above threshold. The relation of g_j and the bias current I can be obtained from the following expression [14]

$$g_j=v\{\alpha_i+\frac{1}{\Gamma L}[\frac{1}{2}\ell n\frac{1}{R_1\cdot R_2}+\ell n\frac{(s_i^+)^{1/2}-(s_i^-)^{1/2}}{(s_i^+)^{1/2}+(s_i^-)^{1/2}}]\} \qquad (21)$$

where α_i is the loss in the cavity, $\alpha_i \cong 10cm^{-1}$ R1=R2$\cong$0.3. s_i^+ and s_i^- are the power of the undulated part of the ith mode at the upper and lower envelope respectively.

Under the threshold, the optical intensity is very weak. For the steady state, the relation between the carrier density and the injected current can be obtained from (8)

$$n=\tau_s j/ed \qquad (22)$$

The values of a' and n_t can be determined from the relation of g_i~I and equations (10), (22). $\Delta\lambda$ was measured from the spontaneous emission spectrum. The photon lifetime can be obtained by

$$\tau_p=[v(\frac{1}{2L}\ell n\frac{1}{R_1\cdot R_2}+\alpha_i)]^{-1} \qquad (23)$$

The values of M_i were calculated from the longitudinal mode spectrums at different bias current. M_i', M_i'' and M_i''' were obtained by a cubic spline fit. The modulation index m, the peak value of the first and the second harmonic were measured at the different bias current. When the second harmonic is the maximum

value,

$$S_j'''(J)=0 \qquad (24)$$

The nomalized current J_p at the peak value of the second harmonic and the spontaneous emission factor C_p were determined from a self -consistent solution of equations (20) and (24). the method can be described as the following: for a given C_p value, a corresponding J_p can be obtained from equation (24); then substituting this J_p into (20), and a new C_p was calculated; continuing this process until c_p and J_p converged to a self-consistent pair. Based on the relation between J_p and correlative bias current, the value of J at the different bias currents was is easy to obtain. then the spontaneous emission factor was calculated from equation (20). The above obtained relation between the spontaneous emission factor and the bias current was taked as a preliminary value. For the spontaneous emission factor at the diffrent bias current,a smoothed curve was set by a cubic spline fit. Then one consideres that both M_p and C_p are the function of the bias current. The following expression can be obtained from (13).

$$f'(J)=1+NeM_p'+Y_o/W \qquad (25)$$

$$f''(J)=NeM_p''+Z_o/W-Y_o^2/W^3 \qquad (26)$$

$$f'''(J)=NeM_p'''+G_o/W-3Y_oZ_o/W^3+3Y_o^3/W^5 \qquad (27)$$

where

$$G_o=2C_p(M_p'''J+3M_p'')+6C_p(M_p''J+2M_p')+6C_p''(M_p'J+M_p)$$
$$+2M_pJC_p'''-NeM_p'''(Q-J+NeM_p)+3M_p''(1-2Ne)(1+NeM_p')$$

$$Z_o=2C_p(M_p''J+2M_p')+4C_p'(M_p'J+M_p)+2M_pJC_p''-NeM_p''(Q-J-NeM_p)+(1+NeM_p')^2$$

$$Y_o=2C_p(M_p'J+M_p)+2M_pJC_p'-(1+NeM_p')(Q-J-NeM_p)$$

Inserting equations (25),(26) and (27) into (17),(18) and(19). and using a method which is similar to the above, new values of J_p and C_p were obtained from the self-consistent solution of equations (20) and (24). Then the spontaneoues emission factors at different bias current were caculated from (20). The cubic spline fit was made again for the new spontaneous emission factors, continuing this process until the curve of the spontaneous emission factor versus the bias current is approximately same in two successive caculations.

In order to measure the spontaneous emission factor of the ith mode the laser is biased at the second harmonic peak of ith mode, then the values of the first and second harmonics, and modulation index were measured, M_p, M_p', M_p'' and M_p''' can be caculated. The spontaneous emission factors of the different mode can be obtained from a self-consistent solution of equations (20) and (24).

B. Experimental Results

The way to measure the first and second harmonic, m etc is the same [8]. In order to measure these values conveneitly and accurately, lasers were selected to have small threshold currents, wide longitudinal spacing and good thermal stability .To reduce the measurement error due to the wavelength change caused by the modulation signal, one could adjuste the exit slit

of the monochromator to make it wider than the entrance slit. Here the width of the entrance slit is 20μm, and the exit slit is 60μm. The frequancy of the modulation signal is 40KHz.

Fig.5 Experiment results, the spontaneous emission factor of the main mode against the bais current for the laser SM1.

Fig.5 illustrates the experimental reselts. The laser SM1 has the cavity length of about 150μm, the active layer thickness of 0.3μm, a longitudinal spacing of 5Å, the gain spectral width of 170Å wavelength of the main mode being 8170Å, and the threshold current of 41.3mA, In Fig.5 , the curve of the spontaneous emission factor against the bias current is the same as the above numerical results. Several devices were measured and the results are the same.

For the laser SM1, the experimental results for the spontaneous emission factors of different modes are listed in Table.1. One can find from Table.1 that the difference between the spontaneous emission factor of the main mode and its neighbouring mode is small. This is in agreement with [8]. But the difference between the spontaneous emission factors of the main mode and the side mode which is far from the main mode is large. The spontaneous emission factor of the -7th side mode is 10 times as smaller as that of the main mode.

Several InGaAsP BH lasers operating at 1.3μm wavelength were measured. The results show that its spontaneous emission factors are about the order of 10^{-4}, and the 10 times as larger as that of AlGaAs lasers. This is in agreement with the numerical results.

TABLE.1
Spontaneous Emission Factor of the Different Mode for the Laser SM1

ℓ	Bias Current(mA) of the Second Harmornic Peak	M_ℓ	C_ℓ
2	40.6	11.6	0.92×10^{-5}
1	41.0	10.1	1.11×10^{-5}
0	41.3	9.07	1.25×10^{-5}
-1	41.2	10.2	1.04×10^{-5}
-2	40.9	12.5	0.89×10^{-5}
-7	40.5	41.6	1.12×10^{-6}

IV. DISCUSSION

The above numerical calculation and the experimental results show that the spontaneous emission factor of the DH laser increases quickly as the injected current increases in a small region under the threshold, and outside this region, the variation of this factor with the injected current is small. According to numerical results ,the large variation of the spontaneous emission factor in the small region under the threshold is mainly due to that the spontaneous emission spectral width decreases quickly as the injected current increases , and the variation of K, $\bar{n}_1$, $\bar{n}_2$, $\bar{n}_3$, $\bar{N}m$, Ve etc. is very small, when the injected current changes.

In Table.1, the difference between the spontaneous emission factors of the main mode and the -7th side mode is large. This is because the M value of the -7th side mode is larger than that of the main mode.

Both numerical and experimental results show that the spontaneous emission factor of the InGaAsP BH laser operating at 1.3μm wavelebgth is about an order larger than that of the AlGaAs stripe geometry laser. This is because the value of the spontaneous emission factor is proportional to λ^4 ,and the difference of the astigmatism factor between the the InGaAsP BH laser and the AIGaAs stripe geometry laser operating at the fundamantal mode is not too large.

V. CONCLUSION

The spontaneous emission factor of semiconductor lasers is closely related with the laser's dimension, waveguide mechanism, working condition etc. For the stripe geometry laser, the shorter the cavity length, and the narrower the stripe width, then the larger the spontaneous emission factor is. The spontaneous emission factor has a maximum value at the thickness of the active layer being about 0.2μm .In a small region under the threshold, the spontaneous emission factor increases quickly as the injected current increases, and outside this region,the variation of this factor is small. The difference between spontaneous emission factors of the main mode and the neighbouring mode is small. But there is a large difference between the spontaneous emission factors of the main mode and the side mode which is far from the main mode. The spontaneous emission factor of the InGaASP BH laser is larger than that of the AlGaAs stripe geometry laser

REFERENCES

[1] R.Salath, C.Voumard and H.Weber, Opto-Electronics,Vol.6, PP. 451-463, 1974.
[2] P.M.Boer, M.T.Vlaardingerbroek, and M.Danielsen, Electron lett., Vol. 11, PP.206-208, May 15, 1975.
[3] K.Petermann, OPt. Quantum Electron., Vol. PP. 233-242, May 1978.
[4] Y.Suematsu and K.Furuya, Trans. IECE Japan, Vol. E60, PP.467-472, Sept. 1977.
[5] K.Petermann, IEEE J.Quantum Electron., Vol. QE-15, PP. 566-570, 1979.
[6] Yiguang Zhao, and Changzhi Guo " The astigmatism factor for semiconductor injection laser" to be published.
[7]. Y.Suematsu, S.Akiba and T.Hong, IEEE J.Quantum Electron., Vol. QE-13, PP. 596-600,1977.
[8] J.C.Goodwin and B.K.Garside, IEEE J.Quantum Electron.,Vol. QE-18, PP.1264-1271, 1982.
[9] Kuo-Lianag Chen and Shyn Wang, IEEE J.Quantum Electron.,Vol. QE-19, PP. 1354-1355, 1983.
[10] M.Yamada, K.Hagano, H.Ishiguro and Y.Suematsu, Jap. J.Appl. Phys., Vol. 18, No.8, P.1513,1979.
[11] H.C.Casey, Jr, and M.B.Panish, Heterostructure Laser, New Youk: Academic Press, 1978.
[12] L.W.Casperson, J.Appl. Phys., Vol. 46, No.12, P.5194,1975.
[13] K.Petermann, Opt. Quantum electron., Vol. 10. P.233, 1978.

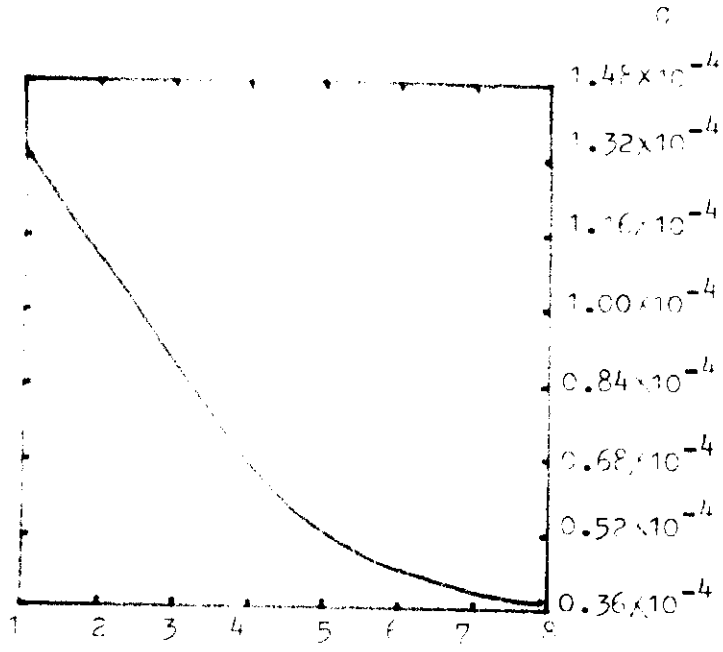
C
1.48×10⁻⁴
1.32×10⁻⁴
1.16×10⁻⁴
1.00×10⁻⁴
0.84×10⁻⁴
0.68×10⁻⁴
0.52×10⁻⁴
0.36×10⁻⁴
1
2
3
4
5
6
7
8
Sw, μm

Fig.1

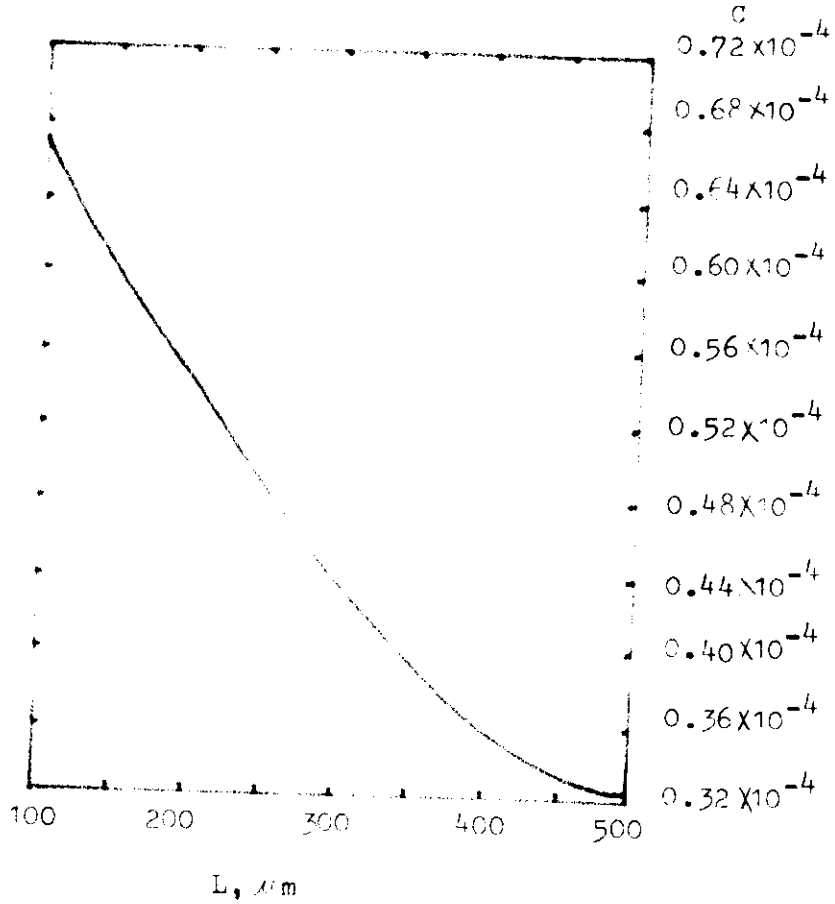
C
0.72×10⁻⁴
0.68×10⁻⁴
0.64×10⁻⁴
0.60×10⁻⁴
0.56×10⁻⁴
0.52×10⁻⁴
0.48×10⁻⁴
0.44×10⁻⁴
0.40×10⁻⁴
0.36×10⁻⁴
0.32×10⁻⁴
100
200
300
400
500
L, μm

Fig.2

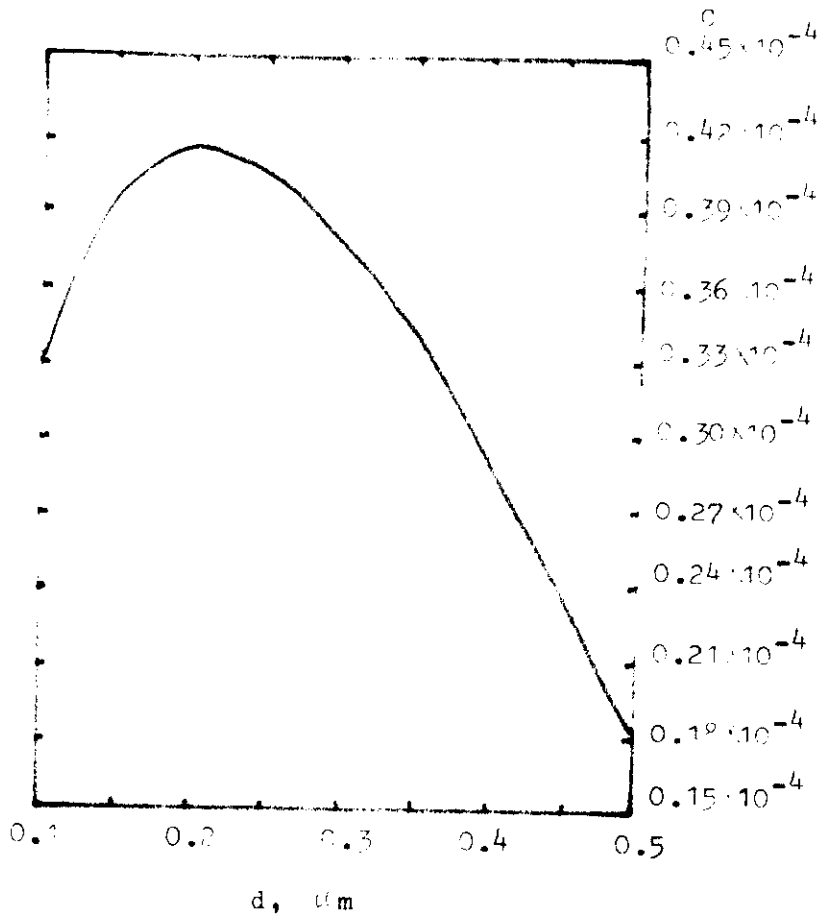
C
0.45×10⁻⁴
0.42×10⁻⁴
0.39×10⁻⁴
0.36×10⁻⁴
0.33×10⁻⁴
0.30×10⁻⁴
0.27×10⁻⁴
0.24×10⁻⁴
0.21×10⁻⁴
0.18×10⁻⁴
0.15×10⁻⁴
0.1
0.2
0.3
0.4
0.5
d, μm

Fig.3

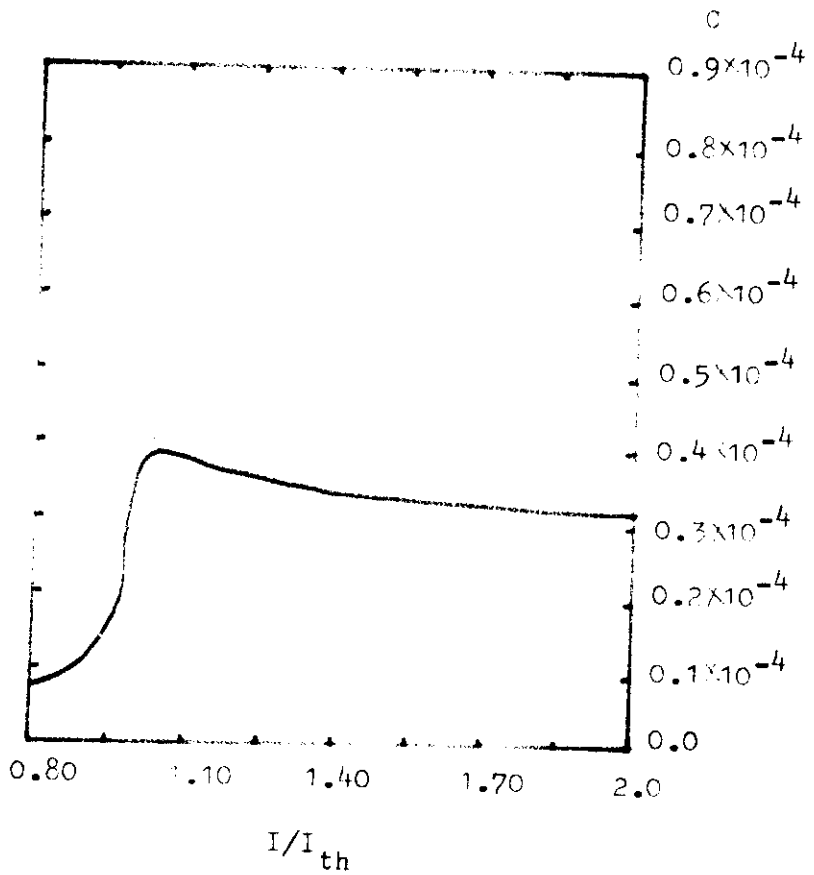
C
0.9×10⁻⁴
0.8×10⁻⁴
0.7×10⁻⁴
0.6×10⁻⁴
0.5×10⁻⁴
0.4×10⁻⁴
0.3×10⁻⁴
0.2×10⁻⁴
0.1×10⁻⁴
0.0
0.80
1.10
1.40
1.70
2.0
I/I th

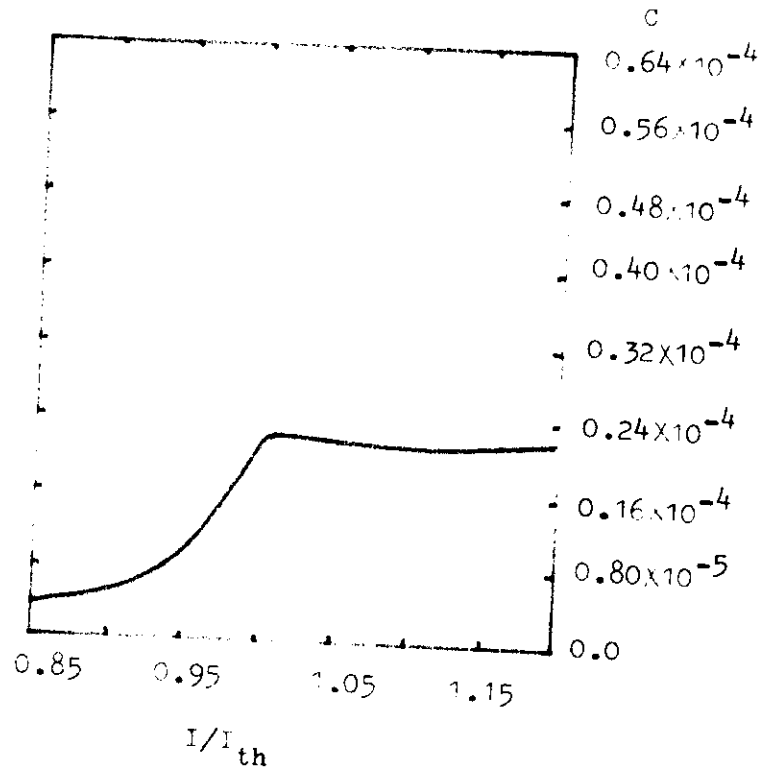
C
0.64×10⁻⁴
0.56×10⁻⁴
0.48×10⁻⁴
0.40×10⁻⁴
0.32X10⁻⁴
0.24X10⁻⁴
0.16×10⁻⁴
0.80X10⁻⁵
0.0
0.85
0.95
1.05
1.15
I/I th

Fig.5

Frequency-Offset Locked Semiconductor Laser Diodes With High Stability Used In Coherent Optical Fiber Communication

Jia Quan Xie Linzhen

Dept. of Radio-Electronics, Peking University
Beijing, China.

ABSTRUCT

Two laser diodes have been stably frequency-offset locked together. The IF frequency (beat frequency) of these two laser diodes is 900 MHz and the beat frequency fluctuation is less than 10 KHz. The system can stably run for more than 24 Hours without any difficulty and has been applied into coherent optical fiber communication systems already. (The measured IF frequency linewidth is 22 MHz).

An IF frequency stablization system with high stability has been built. The experimental set-up is shown in Fig.1. The lasing wavelength of the transmitter and local laser are all 0.824nm, and their models are HLP-1400.
The beat frequency (IF frequency) of these two lasers is 900 MHz or 1.0 GHz and the linewidth of IF signal is less than 22 MHz. The beat signal is detected by a APD (Model PD 1002) and amplified by a preamplifier. The error signal coming out from the dis--criminator is amplified by a PID (Propotional Integrator-Differ--entiator) circuit and fed back into the local laser to sta-blize the beat frequency. The loop time and loop gain are 16μs and 10^6 respectively. The measured IF frequency fluctuation is less than 10KHz and the system can stably run for more than 24 hours without any difficulties.

Fig.2 shows the waveforms of 900 MHz IF frequency signal, and the réduction of IF frequency fluctuation by the feedback loop of this system is shown in Fig.3 (a),(b).

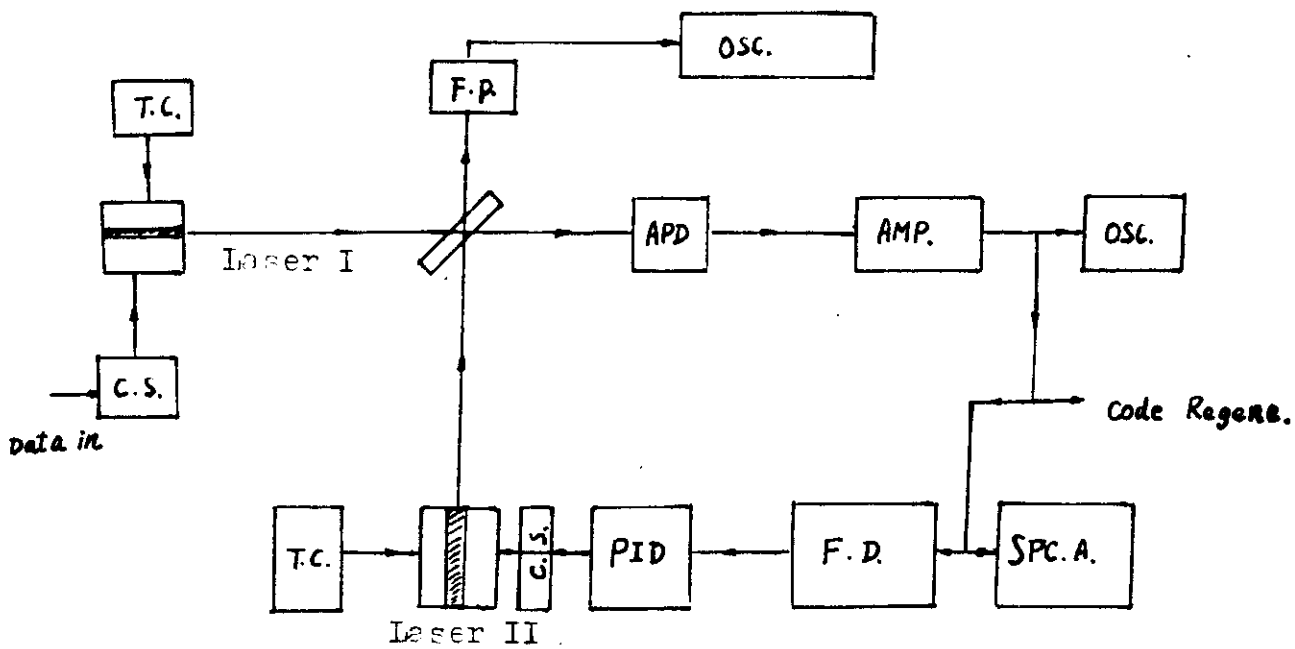

Fig. 1. Experimental set-up. T.C.-Temperature Controller, C.S.-Current Supply, APD-Avalanche Photodetector, F.P.-Fabry-Perot Interferometer, OSC-Oscillascope, AMP-Amplifier, F.D.-Frequency Discriminator, SPC.A.-Spectum Analyzer.

Fig. 2 Waveforms of 900 MHz IF frequency

(a) Free-running

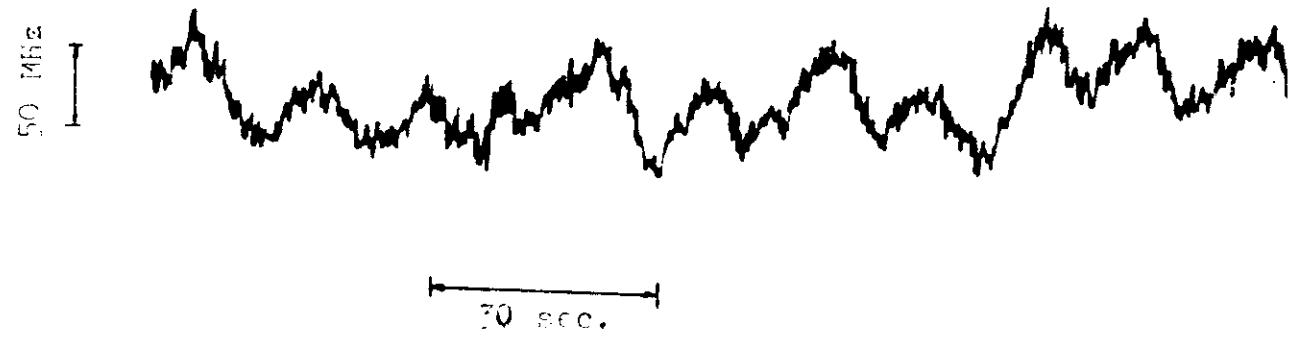

(b) Closed-loop

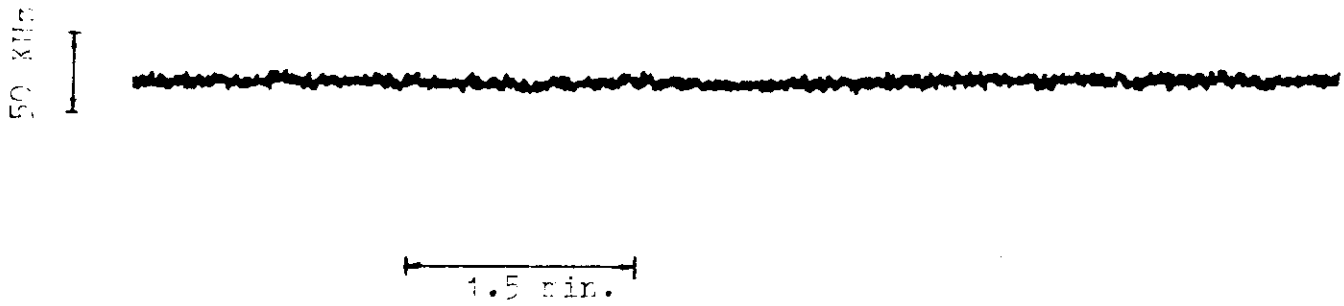

Fig. 3 (a), (b) IF frequency fluctuation reduction by feedback loop

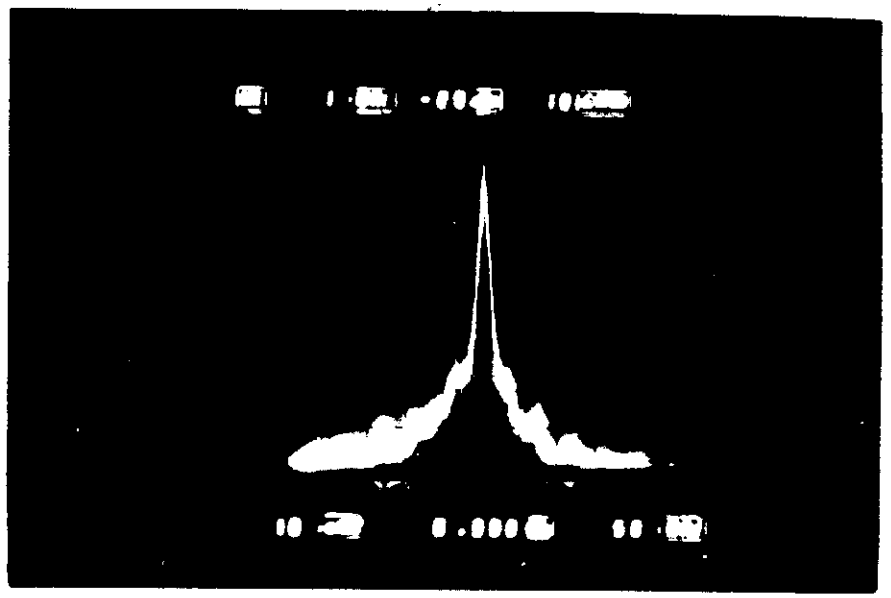

Fig. 3. IF Frecuency Spectrum. The linewidth of IF frecuency is 22 MHz. Horizontal Scale: 50 MHz/Div..

Si Heat Sink and Optical Fibre Mount

CUI Xiao Ming

Department of Physics, PeKing University, Beijing, China

1. Introdution

The simeconductor heterojunction laser is commonly mounted on the copper heat sink (Fig. 1a). The stress may result from bonding process because of the different thermal expansion coefficients of Si and GaAs. And so Indium is commonly used for bonding laser chips on Cu heat sink in order to avoid the stress. The bonding material In will suffer a deterioration due to the oxidation process, especialy the heat generated from the laser will accelerate this process. This process will result in a degeneration of the laser and in turn the reliability of the optical fibre communication system. By using silicon wafer as the heat sink of the laser, the more stable bonding material, such as Au/Sn can be used instead of "soft" In, because the thermal expansion coefficient of Si is very closed to GaAs ($\alpha_{Si}=4\cdot10^{-6}℃^{-1}$ $\alpha_{GaAs}=6\cdot10^{-6}℃^{-1}$ $\alpha_{Cu}=17\cdot10^{-6}℃^{-1}$). The Si heat sink structure is shown in Fig.1b.

Using Si as heat sink gives another advantage. As we know, the Si microfabrication technologies have been well developed. We can utilize the charateristics of preferentially etching on Si for making V groove as a support of optical fibre, which

collects the light emitted from the laser chip mounted on Si heat sink (Fig.2). Because laser and fibre are put on the same Si wafer, the optical alignment between them is easily worked out by simply controling the V groove depth, then the stability and reliability of the device are remarkably improved.

2. Si heat sink technology and measurment of device thermal resistance

At first, Si wafer is metallized. The wafer thickness is about 150um. After cleaning, both sides of Si wafer are in turn evaporated Cr(~500Å) and Au (~2000Å), then it is alloyed at about 450-500 °C. Sn or Sn/Au is evaporated or electroplated to finish the metallization of Si wafer. Finally, the metallization Si wafer is cut into chips to be used as laser heat sink.

The laser chip with P-side down is now mounted on Si heat sink covered with Sn or Sn/Au and then heating up in vacuum to about 300°C for soldering. Then Si heat sink together with the laser chip is mounted on Cu heat sink using Sn/Pb solder and N-side of the laser is wired. Finally, the laser device is fitted on top of the transistor mount.

The use of Si heat sink offers several advantages as mentioned above. However, the thermal conductivity of Si is lower than that of Cu (σ_{Cu}=4W/cm·K , σ_{Si}=2.5W/cm·K), so that using Si heat sink will increace the device thermal resistance. Numerical calculation[1]

on total thermal resistance gives about 42 °C/W and 22 °C/W for GaAlAs-GaAs laser mounted on Si/Cu heat sink and Cu heat sink, respectively (Fig.3). The penalty for using Si as compared to Cu, is about 20 °C/W. We have measured the on both Si/Cu and Cu heat sink. The stripe width and cavity lenth of the laser chips used are 12μm X 300μm.

According to the measurment for first group of 7 laser devices mounted on Si/Cu heat sink, their thermal resistance varys from 30 to 38 °C/W. Another group of 10 laser devices mounted on Cu heat sink gives thermal resistance varying from 19 to 23 °C/W. Comparing to the numerical calculation, the experimental data are smaller, due to the wider strips width of laser. Furthermore, we believe that the smaller thickness of Si heat sink (150μm) also contributes to the reduction of the device thermal resistance.

These measurments show that Si heat sink increaces really the device thermal resistance, but results in no significant effect on the lifetime of the device with low threshold current. For example, the laser threshold current $\lesssim$ 25mA, consuming power o.o5W, then the increase of active region temperature is about $R_T \cdot P \sim 1$ °C, that means the extra temperature elevation of the junction associated with Si heat sink is negligible. In other words, the Si/Cu composite heat sink structure is suitable for laser with low threshold current.

3. Fabrication of Si heat sink with V groove[2]

As we know, the etching rate is much greater in the <100> direction than that in the <111> direction. This anisotropic etching of Si results in a V groove with an angle of 70.53° (Fig.4).

The steps of fabricating V-groove is shown in Fig.5:

1. The wafer with 150μm thick is prepared and cleaned.

2. SiO_2 film of 1μm thick is deposited on the wafer surface.

3. The photolithographic processing, including coat with positive photoresist, exposure and development.

4. The chemical etch with hydrofluoric acid solution ($HF + H_2O$) leaving open windows of SiO_2 film to form oxide mask.

5. The remanining photoresist is removed, then the wafer is placed into potassium hydroxide solution ($KOH + H_2O$) for etching V-groove.

6. Finally, the oxide mask is removed, leaving the Si wafer with V-groove.

It is necessary to control groove width and depth to ensure the optical alignment between the laser chip bonded on Si heat sink and the optical fibre mounted in the V-groove. For conventional optical fibre with 125um outer diameter, the width of V-groove is about 147μm and depth about 70μm. Then the optical fibre core is coupled to the luminous region of laser and the efficient coupling can be obtained. In this case, the metallized surface of Si wafer is not only for bonding the laser chip, but also for soldering the fibre if its outer surface is also metallized (Fig.6). Obviously, this coupling technique

is simple and with high precision, comparing to the conventional mechanical adjustment method.

4. conclusion

The use of Si as heat sink material can avoid the stress introduced in bonding process with hard solder and eliminate the degradation due to the use of soft bonding material. Althogh Si heat sink increases the device thermal resistance, but laser life-time is not affected noticeably if threshold is low. Besides , high precision mount for optical fibre for coupling can be made based on Si microfabrication technology. The Si heat sink with V-groove facilitates the optical alignment between the laser and fibre, and provides efficient coupling, simple structure and better device reliability.

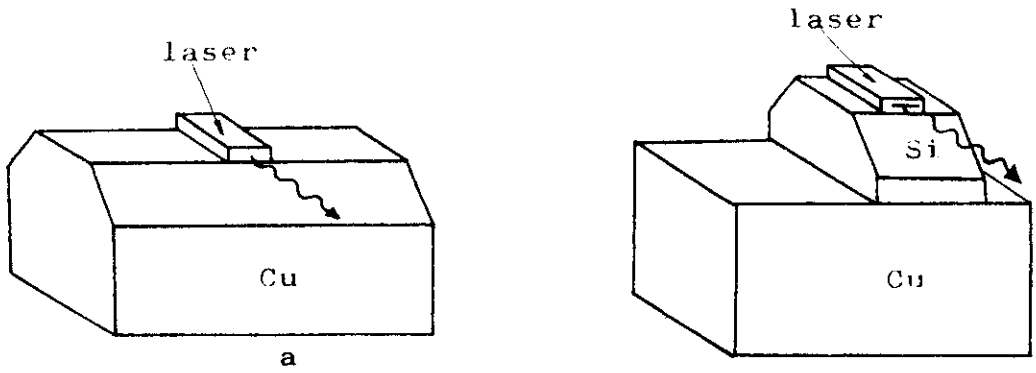

(a) (b)

Fig.1(a) Laser mounted on Cu heat sink

(b) Laser mounted on Si/Cu heat sink

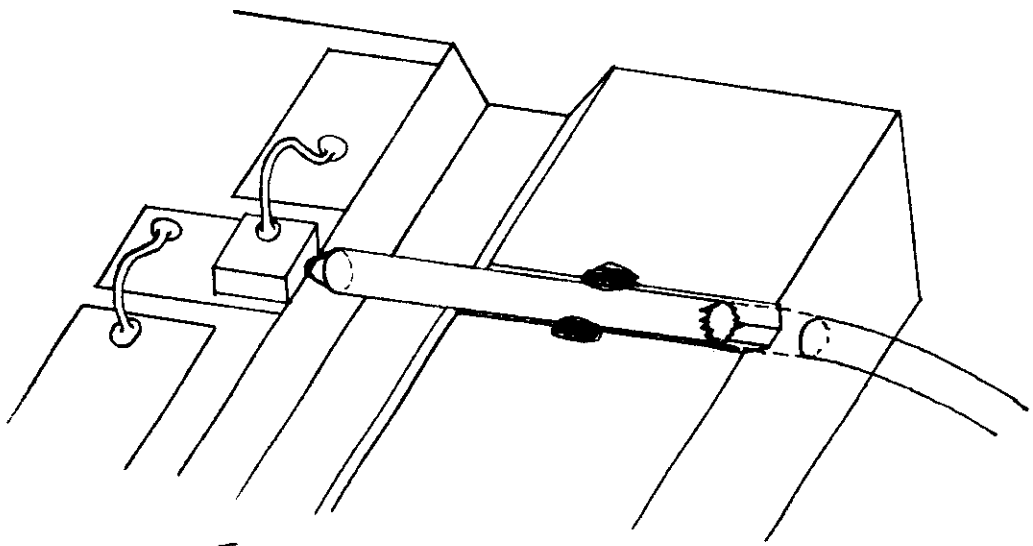

Fig.2

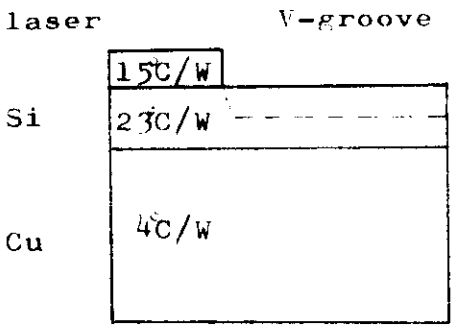

Fig.3 Thermal resistance distribution of laser mounted on Si/Cu heat sink. The Si sub-mount is of 200μm, and laser strip width is 6μm.

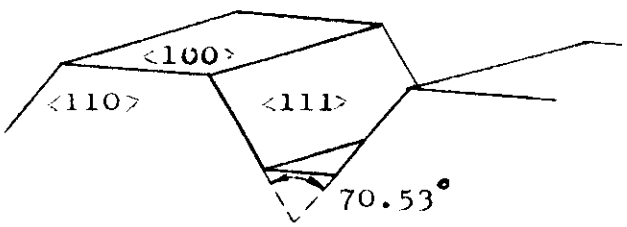

Fig.4 V-groove geometry

100

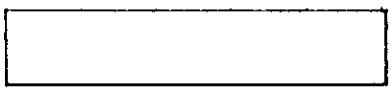

(a). Cleaning

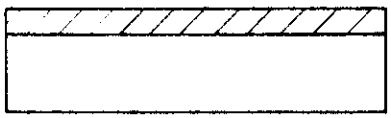

(b) Oxide film is deposited

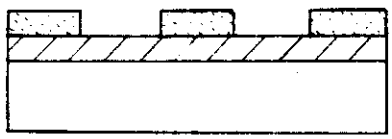

(c) Photolithographic processing

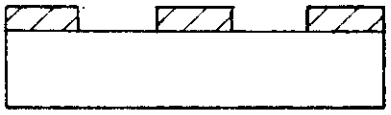

(d) Etch forming oxide mask

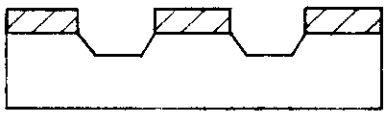

(e) Etch V-groove in substrate

(f) Remove oxide mask

Fig.5 Fabrication process of V-groove

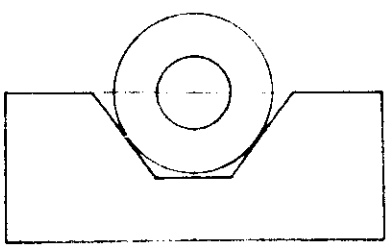

Fig.6

REFERENCES

1. EUGENE DUDA, JEAN CLAUDE CARBALLES, AND JACQUES APRUZZESE, "Thermal Resistance and Temperatur Distribution in Double-Heterostructure Laser: Calculations and Experimental Results" IEEE, JOURNAL OF QUANTUM ELECTRONICS, 1979, VOL. QE-15, No.8, P.812.

2. C.M.SCHROEDER. "Accurate Silicon Spacer for an Optical Fibre Cable Connector" THE BELL SYSTEM TECHNICAL JOURNAL, JANUARY 1978, VOL.57, No.1, P.91.